Structural Analysis

G. Roth

This document has been published in

Thomas Brückel, Gernot Heger, Dieter Richter, Georg Roth and Reiner Zorn (Eds.):
Lectures of the JCNS Laboratory Course held at Forschungszentrum Jülich and the research reactor FRM II of TU Munich
In cooperation with RWTH Aachen and University of Münster
Schriften des Forschungszentrums Jülich / Reihe Schlüsseltechnologien / Key Technologies, Vol. 39
JCNS, RWTH Aachen, University of Münster
Forschungszentrum Jülich GmbH, 52425 Jülich, Germany, 2012
ISBN: 978-3-89336-789-4

8 Structural Analysis

G. Roth
Institute of Crystallography
RWTH Aachen University

Contents

8.1 Introduction 2

8.2 Diffraction Contrast Variation 2

8.3 The hydrogen problem in structural analysis 4

8.4 Atomic coordinates and displacement parameters 7

8.5 Magnetic structures from neutron diffraction 9

8.6 Electron densities from x-rays and neutrons 12

8.7 Magnetization densities from neutron diffraction 14

References 15

Exercises 16

Lecture Notes of the JCNS Laboratory Course Neutron Scattering

8.1 Introduction

The analysis of crystal structures and magnetic ordering is usually based on diffraction phenomena caused by the interaction of matter with x-rays, neutrons or electrons. Even though modern electron microscopy (HRTEM) can achieve atomic resolution, more detailed and quantitative information on the 3D atomic arrangement in crystals and on 3D magnetic structures and spin densities requires diffraction methods. In a more general nomenclature, diffraction is equivalent to coherent, elastic scattering. The basic theory of diffraction used for structural analysis (the so called kinematical theory) is similar for all types of radiation. Due to the different properties of x-rays, neutrons and electrons and their specific interaction with matter, complementary information is obtained from experiments with different types of radiation.

Considering only x-rays and thermal neutrons one finds that their wavelengths are similar (0.5 Å < λ < 2.4 Å) but they are scattered very differently by matter: While the electromagnetic x-radiation is scattered from the electrons and yields the total electron density distribution in the crystal, the nuclear scattering of neutrons is sensitive to the density distribution of the nuclei and the magnetic neutron scattering probes the magnetisation density of unpaired electrons.

x-ray diffraction using conventional laboratory equipment and/or synchrotron installations is the most frequently used method for structure analysis. Neutrons are, however, indispensable in a number of applications. The purpose of this chapter is to discuss a few typical examples of structural analysis, for which, instead of or complementary to x-rays, neutrons are required to solve structural problems.

8.2 Diffraction Contrast Variation

A great advantage of neutrons over x-rays in the context of structural analysis is the very much different variation of the scattering length of atoms within the periodic system of the elements: The contrast in conventional x-ray diffraction is directly related to the ratio of the number of electrons Z_j of the different atoms or ions j involved. The atomic scattering factor f_j in the structure-factor formula, which represents the Fourier transform of the atomic electron density distribution, is proportional to Z_j ($f_j = Z_j$ for $\sin\theta/\lambda = 0$). Standard x-ray techniques can hardly differentiate between atoms/ions with a similar number of electrons (like Si and Al or Cr and Mn). Even if the atoms are fully ordered on different sites, x-ray diffraction just ‘sees’ the average structure.
For neutrons the atomic scattering factor f_j is replaced by the nuclear scattering length (or coherent scattering amplitude) b_j, which is of the same order of magnitude for all nuclei but varies from nucleus to nucleus in a non-systematic way. b_j values can be either positive or negative and depend on the isotopes and nuclear spin states of the element j (see chapter 4).

Crystal structure and site occupation of $(Mn_{1-x}Cr_x)_{1+\delta}Sb$.

As an example of contrast variation, the combination of x-ray and neutron diffraction information is demonstrated for the intermetallic compounds $(Mn_{1-x}Cr_x)_{1+\delta}Sb$, with $0 \le x \le 1$ [1]. This solid solution system is interesting for its magnetic properties: One end member of the solid solution series ($Mn_{1+\delta}Sb$) shows isotropic ferromagnetic behaviour while the other one ($Cr_{1+\delta}Sb$) is a uniaxial antiferromagnet. Intermediate compositions are characterized by competing magnetic interactions leading to a complex magnetic phase diagram. The crystal structure is closely related to the hexagonal NiAs-type structure (space group: $P6_3/mmc$) with some additional partial occupation (≤ 0.14) of the interstitial site 2(d) (see Fig. 8.1):

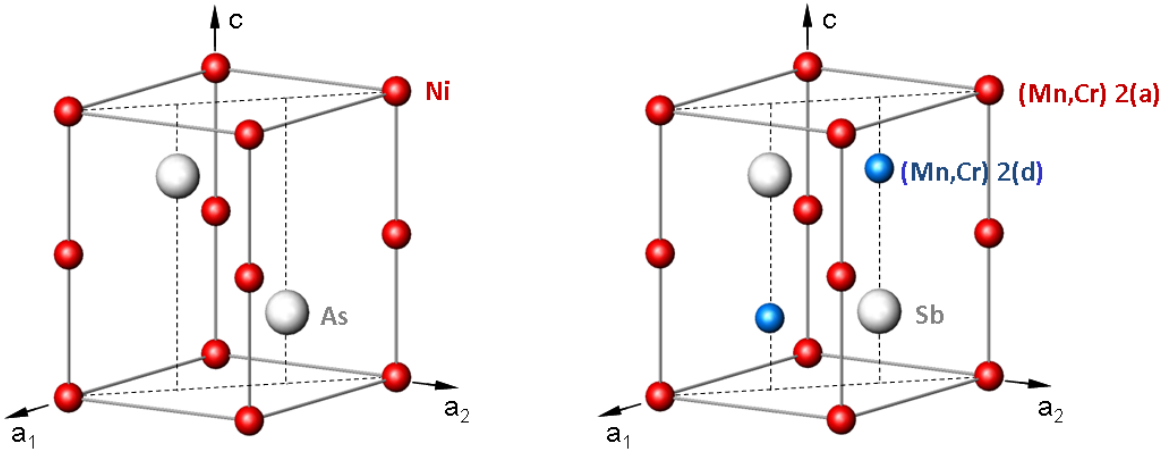

Fig. 8.1: *Left: NiAs structure, right: $(Mn_{1-x}Cr_x)_{1+\delta}Sb$ structure*

Conventional x-ray diffraction can hardly differentiate between chromium (Z_{Cr}= 24) and manganese (Z_{Mn}= 25) but still yields information on the overall occupation probabilities by (Mn,Cr) for site 2(a) (denoted as a) and site 2(d) (denoted as d). The Sb position is assumed to be fully occupied, thus serving as an internal standard for the scattering power.
The compound formula can now be reformulated site-specifically as:

$$\underset{\textit{site 2(a)}}{(Mn_{1-y}\,Cr_y)_a}\;\underset{\textit{site 2(d)}}{(Mn_{1-z}\,Cr_z)_d}\;Sb$$

corresponding to a chemical composition of $Mn_{[(1-y)a\,+\,(1-z)d]}\,Cr_{[ya\,+zd]}\,Sb$.

On the other hand, the nuclear scattering lengths of Cr and Mn for neutron diffraction are extremely different with b_{Cr} = +3.52 fm and b_{Mn} = -3.73 fm (see also chapter 4).
In the structure analysis of the neutron data, site-specific effective scattering lengths b_{eff} (2a) and b_{eff} (2d) are refined, which in turn are expressed as:

$b_{eff}(2a) = a\cdot[(1-y)\cdot b_{Mn} + y\cdot b_{Cr}]$ and $b_{eff}(2d) = d\cdot[(1-z)\cdot b_{Mn} + z\cdot b_{Cr}]$

solving for the unknown parameters y and z gives:

$y = [b_{eff}(2a)/a - b_{Mn}] / [b_{Cr} - b_{Mn}]$ and $z = [b_{eff}(2d)/d - b_{Mn}] / [b_{Cr} - b_{Mn}]$.

The combination of the overall occupation probabilities a and d - from conventional x-ray studies – with the effective scattering lengths b_{eff}(2a) and b_{eff}(2d) determined in a neutron diffraction experiment allows the evaluation of the Cr and Mn concentrations on the different sites 2(a) and 2(d).
It is evident, that the individual (Cr,Mn) distributions on the two crystallographically different sites 2(a) and 2(d) are not accessible merely by a chemical analysis. For most of the samples studied, the site 2(a) was found to be fully occupied: a ≈ 1.0. But the formula $(Mn_{1-x}Cr_x)_{1+\delta}Sb$ used normally is only correct for the special case of equal Cr : Mn ratios on both sites:

$$x = y = z \quad \text{and} \quad 1 + \delta = a + d.$$

Note that, in general, a statistical occupation of one crystallographic site with three kinds of scatterers - e.g. Mn, Cr and "vacancies" - requires at least two independent experiments with sufficiently different relative scattering power of the atoms involved to determine the fractional occupancies.
The detailed information on the (Cr,Mn) distribution is needed to explain the magnetic properties of these intermetallic compounds, but we will not further elaborate on this.

8.3 The hydrogen problem in structural analysis

The determination of the structural parameters (coordinates, displacement parameters) of hydrogen atoms in crystals is a special problem involving again the different properties of x-rays and neutrons. It is obvious that H or D atoms with Z = 1 give only a small contribution to the electron density and, therefore, they are hardly visible in x-ray structure analysis, particularly if heavy atoms are also present in the structure. However, there is an even more fundamental problem: The single electron of H or D is engaged in the chemical bonding and is by no means localised at the proton/deuteron position. Therefore, bond distances from x-ray diffraction involving hydrogen are notoriously wrong and any comparison with quantum mechanical calculations is quite hard to perform. This lack of sound experimental information is in sharp contrast to the importance of hydrogen bonding in solids, particularly in biological molecules like proteins, where hydrogen bonds govern to a large extent structures and functionalities of these ‘bio-catalysts’. A combination with neutron diffraction experiments is important to determine the structural parameters of the H/D atoms properly. More generally, the structure analysis by neutron diffraction yields separately and independently from the x-ray data the structure parameters of all atoms including the mean square displacements due to static and dynamic (even anharmonic) effects.

H/D ordering in ferroelectric RbH_2PO_4 (RDP):

The hydrogen problem in crystal structure analysis is of special importance for structural phase transitions driven by proton ordering. KH_2PO_4 (KDP) is the most well-known representative of hydrogen-bonded ferroelectrics. Here, we discuss the isotypic RbH_2PO_4 (RDP). The crystal structure consists of a three-dimensional network of PO_4-groups linked by strong hydrogen bonds (Fig. 8.2).

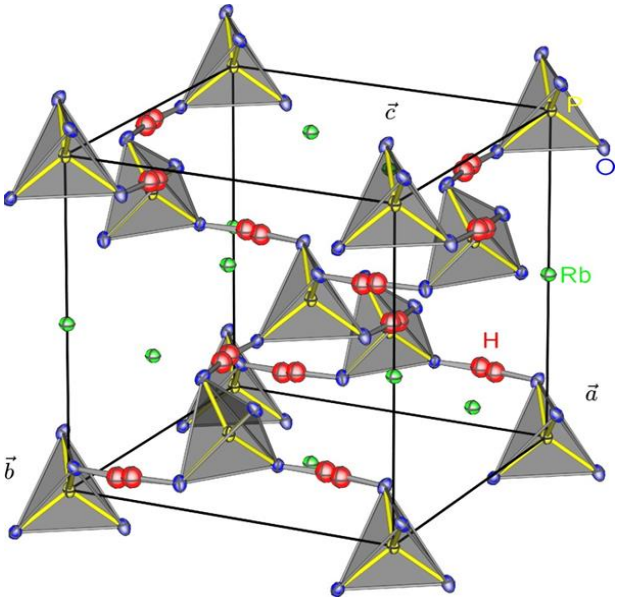

Fig. 8.2: *Crystal structure of the paraelectric phase of RDP (RbH_2PO_4) with a split-model representation of the hydrogen disorder [3].*

In the paraelectric phase at room temperature KDP as well as RDP crystallise in the tetragonal space group I $\bar{4}$2d, where the H-atoms are dynamically disordered in symmetric O···H···O bonds, which are almost linear with short O–O distances, typically in the range of 2.5 Å. The disordered H-distribution may be interpreted as corresponding to a double-well potential [2].
Figures 8.3 and 8.4 show the corresponding results for RDP, obtained from single crystal neutron diffraction [3].

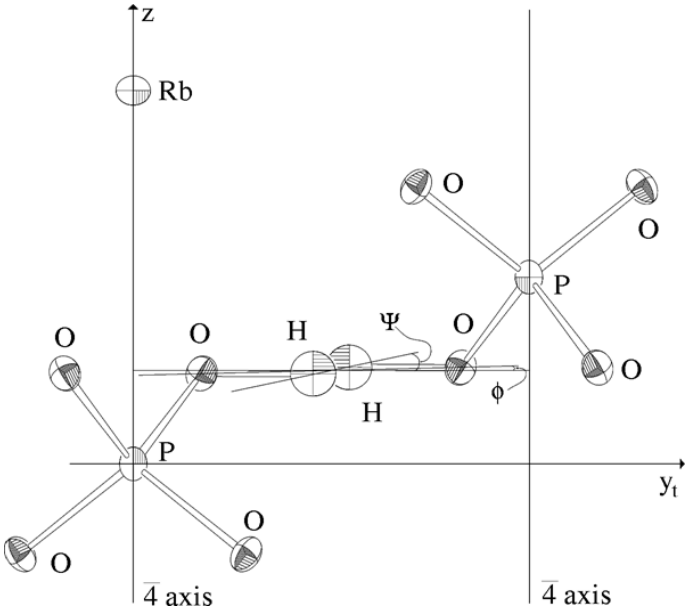

Fig. 8.3: *Local configuration of two PO_4-tetrahedra in the paraelectric phase of RDP (RbH_2PO_4)(at T_c + 4 K) linked by a strong, disordered hydrogen bond [3].*

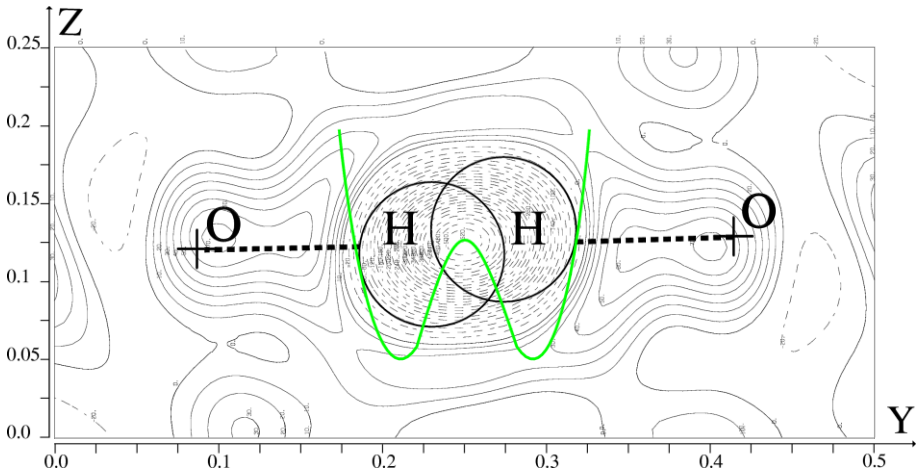

Fig. 8.4: *Difference-Fourier-plot of the negative proton density in the hydrogen bond of paraelectric RDP indicated by broken contour line [3]. The double-well potential model used to describe this density is inscribed in green.*

The two very close hydrogen positions with 50% occupation probability are, of course, an artefact of the time-space averaging that is inherent to diffraction. In this case, the hydrogen disorder is assumed to be a dynamic hopping process between the two energetically degenerate sites.
At T_c = 147 K, RDP transforms to a ferroelectric phase of orthorhombic symmetry (space group: Fdd2) in which the protons order in short asymmetric O-H···O bonds (Fig. 8.5). The PO4-tetrahedra show a characteristic deformation with two shorter and two longer P-O distances due to a transfer of electron density to the covalent O–H bonds. The electrical dipole moments are oriented ||z which give rise to a polarisation along the ***c***-direction.

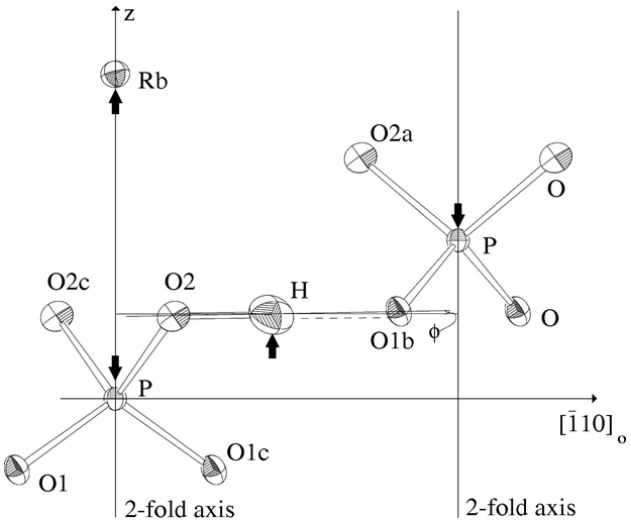

Fig. 8.5: *Ferroelectric, hydrogen-ordered structure of RDP close to the phase transition at T_C – 1 K (major changes indicated by arrows, presentation as in Figure 8.3) [3].*

The phase transition temperatures of KDP-type compounds change drastically when H is substituted by D. For $K(H,D)_2PO_4$, for instance, the para- to ferroelectric T_C changes from 122 K in the protonated to 229 K in the deuterated compound. This huge H/D-isotope effect proves that hydrogen-ordering and -dynamics is the major factor controlling this phase transition. Another type of H/D-isotope effect was found for $Tl(H,D)_2PO_4$ (TDP/DTDP) and $Rb(H,D)_2PO_4$ (RDP/DRDP), where a different polymorphism between the protonated and deuterated phases exists.

Clearly, the use of neutron diffraction is detrimental to a better understanding of these compounds and their interesting physical properties.

8.4 Atomic coordinates and displacement parameters

As discussed above, neutron diffraction is very useful for obtaining precise atomic coordinates and displacement parameters. The improved accuracy (compared to x-rays) stems mainly from the absence of the form-factor fall-off. We will use measurements on Cobalt-olivine, Co_2SiO_4, (crystal size 3 x 2 x 2 mm) taken at the four-circle diffractometer HEiDi at the hot-neutron source of the FRM II reactor (λ = 0.552 Å) for demonstrating this advantage for the thermal displacements:

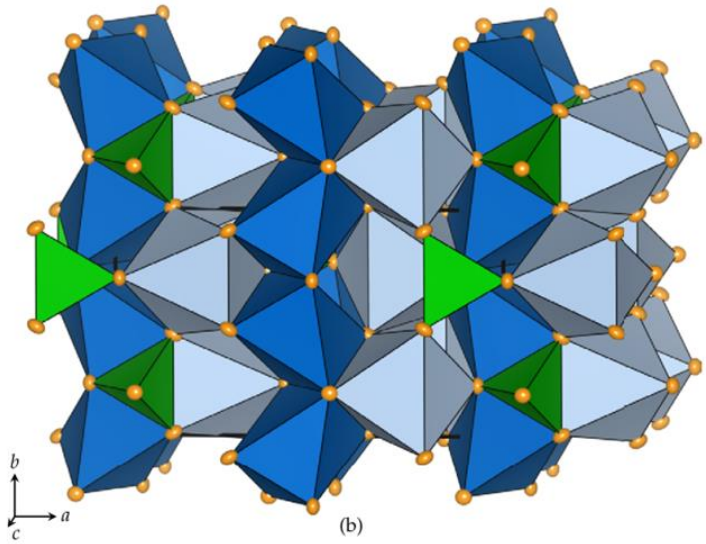

Fig. 8.6: *Structure of Co_2SiO_4 olivine at room temperature, projected along c. Green: SiO_4-tetrahedra, Dark blue: $Co(1)O_6$-octahedra, light blue: $Co(2)O_6$-octahedra. Displacement ellipsoids are plotted at the 95% probability level (from [4]).*

The olivine structure (fig. 8.6) consists of chains of two types of edge-sharing CoO_6-octahedra connected by SiO_4-tetrahedra. A large data set with 1624 independent reflections up to sin θ/λ = 1.05 Å^{-1} had been measured. The data were then successively cut off in shells of sin θ/λ and the resulting partial data sets were used to analyse the displacement parameters. Figure 8.7 shows two interesting observations: First of all, the precision improves significantly with increasing $(\sin \theta/\lambda)_{max}$, as is evident from the decreasing size of the error bars. In the x-ray case, high angle reflections are usually very weak and their measurement does often not lead to improved precision. Secondly, there is a systematic change of the displacement values themselves, resulting from systematic errors that vary with $(\sin \theta/\lambda)_{max}$.

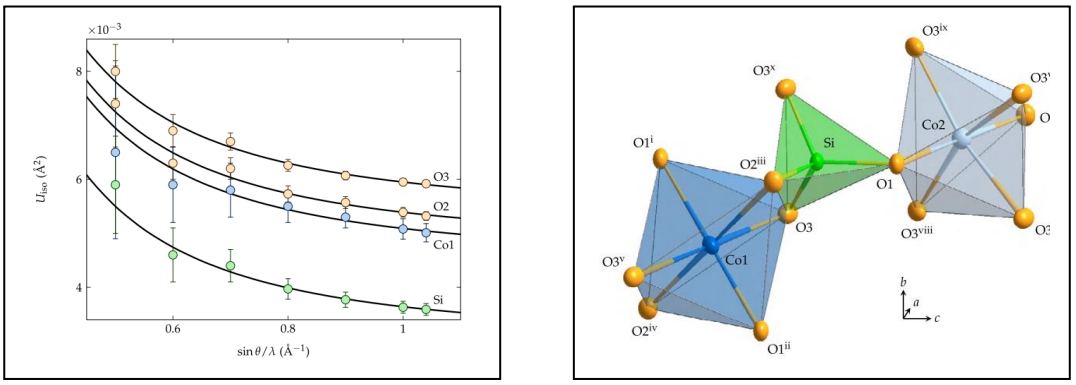

Fig. 8.7: *Left: Statistical (error bars) and systematic errors of isotropic displacements parameters in Co_2SiO_4 as a function of measured sin θ/λ range from single-crystal neutron diffraction data at room temperature [4]. Right:*

Clinographic view of the CoO_6 and SiO_4 polyhedra in Co_2SiO_4 at room temperature [4].

High d_{hkl}-value resolution data from neutron diffraction is also useful to derive precise temperature dependent displacement parameters (fig. 8.8):

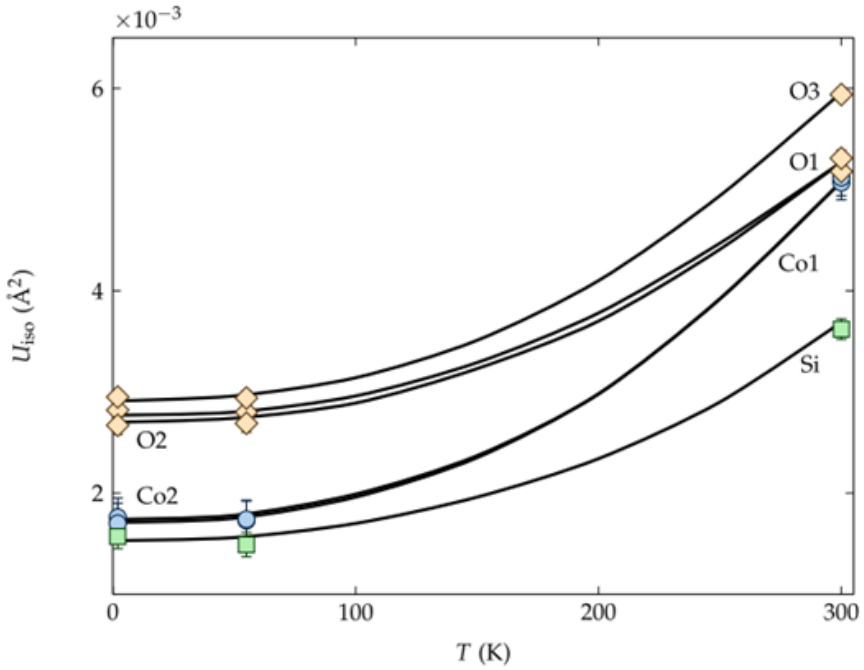

Fig. 8.8: *Temperature dependence of the isotropic displacement parameters of Co_2SiO_4 [4].*

Just as in the case of high quality single crystal x-ray diffraction data, anisotropic displacement parameters can be determined as well. In addition to that, the quality of single crystal neutron data also often allows refining anharmonic displacement parameters. Anharmonic oscillations of atoms in crystals occur if the atoms are vibrating in a non-parabolic potential well. In such cases, the harmonic approximation, which is the basis of the description of thermal displacements by the Debye-Waller factor, fails. Analysis of the anharmonic displacements allows to reconstruct the non-parabolic potential at the site of the vibrating atom.

8.5 Magnetic structures from neutron diffraction

Cobalt-Olivine, Co_2SiO_4, orders magnetically below about 50 K. The magnetic moments of the Co^{2+}-ions turn from a paramagnetic phase with no long range order of the magnetic moments into an antiferromagnetically ordered arrangement. We use Co_2SiO_4 again to briefly demonstrate the application of neutron diffraction to the structural analysis of magnetic structures. This time, a powder neutron diffraction experiment has been performed at the diffractometer D20 (ILL, France) in its high-resolution mode, at temperatures between 70K and 5K, with a neutron wavelength of λ = 1.87 Å and approximately 2 g of powdered Co_2SiO_4 [4].

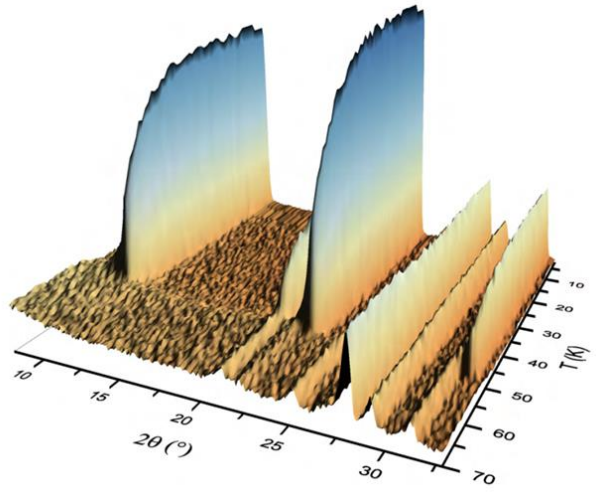

Fig. 8.9: *Thermal evolution of the neutron powder diffraction pattern (low angle part) of Co_2SiO_4 [4].*

At about 50 K, new magnetic reflections (001), (100), (110), (300) etc. appear (fig. 8.9). The nuclear reflections don't change much at the magnetic phase transition. The new reflections can be indexed with the same unit cell as the nuclear reflections, but they were forbidden in the paramagnetic phase with space group P n m a. Obviously, the symmetry has changed at the magnetic ordering transition. The task is then - just as in 'ordinary' structure determination - to find a structural model (that is: magnetic moments and their orientation on the magnetic ions, here Co^{2+}) that fits the observed positions and intensities of the magnetic Bragg peaks. Magnetic structure determination is outside the scope of this chapter, but assumed such a model has been constructed, it can be refined - in the case of powder data by the Rietveld method (fig. 8.10).

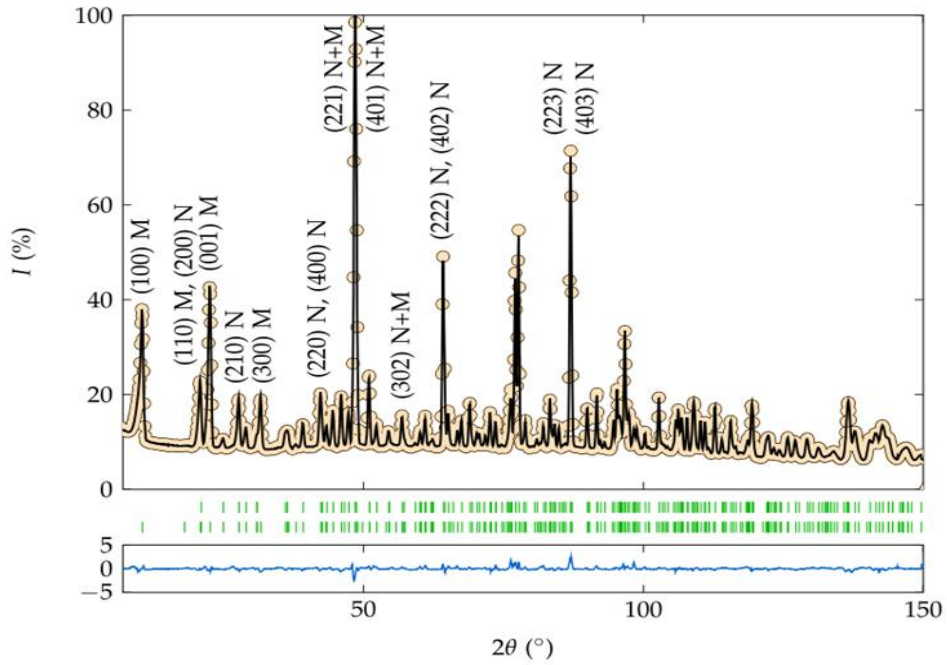

Fig. 8.10: *Neutron powder diffraction pattern (dots), Rietveld fit (black line) and allowed Bragg reflections (green marks) at 5 K of Co_2SiO_4 [4].*

The lower trace (blue) is the difference *Iobs - Icalc* on the same scale. The upper row of the green marks shows Bragg reflections corresponding to the nuclear phase and the lower row represents the allowed positions of the magnetic peaks. Some of the Bragg peaks are indexed. 'N' and 'M' denote the nuclear and magnetic contributions, respectively [4]. Note that the magnetic Bragg peaks are only visible at low diffraction angles.

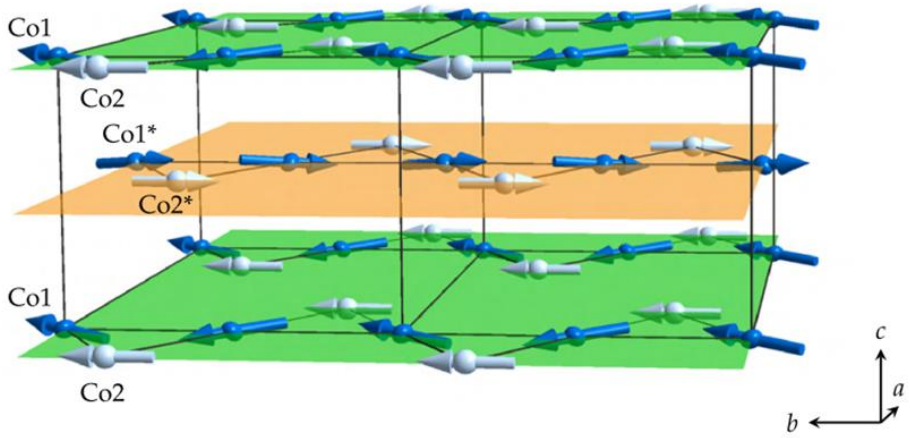

Fig. 8.11: *Graphical representation of the magnetic structure of Co_2SiO_4 below 50 K. The non-magnetic atoms (Si and O) are excluded for simplicity. The figure shows the zigzag chains of Co(1) and Co(2) in layers perpendicular to the c axis [4].*

From the Rietveld refinements, one can derive the exact spin orientation (fig. 8.11) as well as parameters describing quantitatively the magnetic moments on the two symmetrically non-equivalent Co^{2+}-sites (see table below). However, magnetic neutron diffraction from single crystals often gives additional and more accurate information:

	Co1 (0,0,0)	Co2 (x,1/4,z)
M_x (μ_B)	1.18 ± 0.05	—
M_y (μ_B)	3.61 ± 0.04	3.37 ± 0.04
M_z (μ_B)	0.66 ± 0.18	—
M (μ_B)	3.86 ± 0.05	3.37 ± 0.04
ϕ (°)	71.9 ± 0.7	90
θ (°)	80.2 ± 2.7	90

$\chi^2 = 2.23$, $R[F^2 > 2\sigma(F^2)] = 0.033$, $wR(F^2) = 0.044$.

The table shows cartesian (M_x, M_y and M_z) and spherical (M, φ and θ) components of the Co1 and Co2 magnetic moments according to the single-crystal neutron diffraction data at 2.5 K. The directions of the magnetic moments for other cobalt ions in the unit cell can be obtained by applying the symmetry operations of the magnetic space group (Schubnikov group) Pnma.

8.6 Electron densities from x-rays and neutrons

Another advanced application of neutron diffraction in structural analysis is the determination of 3-dimensional high resolution maps of the electron density in the unit cell to study, for instance, details of the chemical bonding. The most involved method of electron density studies (called x-N-synthesis) uses a combination of high quality single crystal neutron and x-ray diffraction experiments. In the present case, a single crystal of Co_2SiO_4 with dimensions 3 x 2 x 2 mm, was measured on the four-circle diffractometer HEiDi at the hot-neutron source of the FRM II reactor (Garching) at λ = 0.552 Å, the single crystal x-ray (synchrotron) experiment was performed on Diffractometer D3 at the synchrotron facility HASYLAB/DESY (Hamburg) with a Co_2SiO_4-sphere, diameter 150 μm as the sample and an x-ray wavelength of λ = 0.5 Å.
The next step is to take the x-ray-data, do a Fourier-transform (Fourier-synthesis) to obtain the electron density map:

$$\rho(\boldsymbol{r}) = 1/V \cdot \sum_{\tau} \boldsymbol{F}(\boldsymbol{\tau}) \cdot \exp[2\pi i(\boldsymbol{\tau r})], \quad \text{with } \boldsymbol{F}(\boldsymbol{\tau}) = |\boldsymbol{F}(\boldsymbol{\tau})| \cdot \exp[i\varphi(\boldsymbol{\tau})].$$

The phases $\varphi(\boldsymbol{\tau})$ are calculated from the atomic model (structure factor equation, see ch. 4), the moduli $|\boldsymbol{F}(\boldsymbol{\tau})|$ are taken from the measured x-ray intensities. The result is a 3-dimensional map of the total electron density $\rho(\boldsymbol{r})$ within the unit cell:

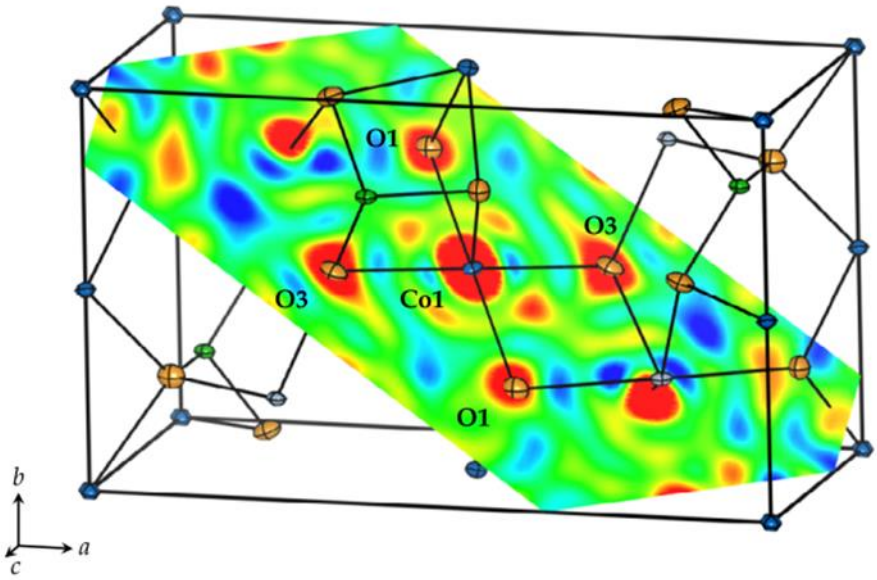

Fig. 8.12: *Electron density distribution $\rho(r)$ of Co_2SiO_4 at 12 K from Fourier synthesis of x-ray data. Contours range from −8 e/Å^3 (blue) to 10 e/Å^3 (red). A plane which intersects the $Co1O_6$ octahedron and contains the Co1, O1 and O3 atoms is shown together with a sketch of the crystal structure [4].*

In favourable cases, such a map already shows interesting features of the (anisotropic) bonding electron density, however, the information content of the map can be very significantly improved by taking the coordinates and displacement parameters from the more accurate neutron diffraction experiment (see above for the reasons) and calculate, in a second step, the so called deformation density. This is done by subtracting from the total electron density $\rho(\boldsymbol{r})$ the density $\rho(\boldsymbol{r})_{spherical}$ corresponding to a superposition of spherical atoms at the nuclear positions. More specifically: atomic positions x_j, y_j, z_j and thermal displacements T_j of atoms j derived from the neutron experiment, 'decorated' with the calculated spherical single atom electron densities.

$\rho(\boldsymbol{r})_{deform} = \rho(\boldsymbol{r}) - \sum \rho(\boldsymbol{r})_{spherical}$, where the sum runs over all atoms in the unit cell.

$\rho(\boldsymbol{r})_{spherical}$ corresponds to the expectation value of the electron density within the unit cell without any effects which are due to chemical bonding. The deformation density then represents the deformation of the charge distribution as a result of the formation of chemical bonds. Figure 8.13 shows such a deformation density map for Co_2SiO_4. In favourable cases, the electron density in the hybridized bonding orbitals (in this case of Co3d- and O2p character) can be directly observed.

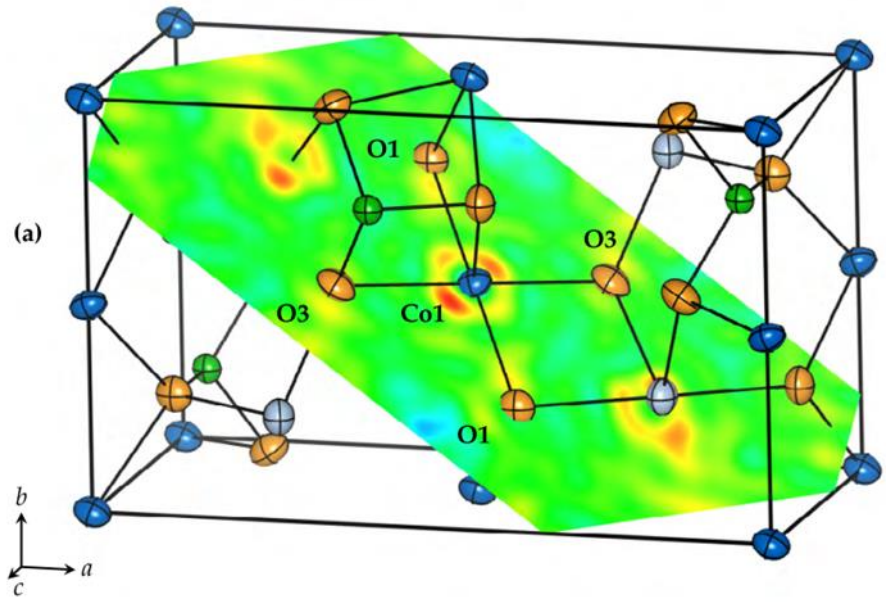

Fig. 8.13: *Deformation density from the x-N-difference Fourier map of Co_2SiO_4 at 300 K: Section through the O1–Co1–O3 plane The difference density varies from −1.25 e/Å^3 (blue) to 1.15 e/Å^3 (red) [4].*

8.7 Magnetization densities from neutron diffraction

As a final example for the application of neutron diffraction in structural analysis, we briefly sketch how a 3-dimensional map of the magnetization density, that is: the density of magnetic moments (spin- as well as orbital-moments) within the unit cell can be determined. These maps are sometimes lucidly called 'spin density maps', but in systems with non-vanishing orbital moments, the term magnetization density is really the correct one.

The experiment is performed by polarized neutron diffraction on a single crystal using the flipping ratio method For details on the experimental method see the chapter on magnetic scattering. The flipping ratio method allows to separate nuclear and magnetic contributions to the diffracted intensities. It is performed *above* the magnetic phase transition in the paramagnetic state (in the case of Co_2SiO_4 above T_N=50K) and the sample is in a strong external magnetic field (here: 7 T). 207 Bragg reflection flipping ratios were measured at diffractometer 5C1 of the ORPHÉE reactor (Laboratory Léon Brillouin, CEA Saclay, France) for Co_2SiO_4 at 70K up to sin $\theta/\lambda \approx 0.62$ Å^{-1} at a neutron wavelength of λ = 0.845 Å. Given the flipping ratios and the nuclear structure factors, the magnetic structure factors can be calculated which are then Fourier transformed to give the spatially resolved magnetization density shown in figure 8.14 in a section through the unit cell of Co_2SiO_4.

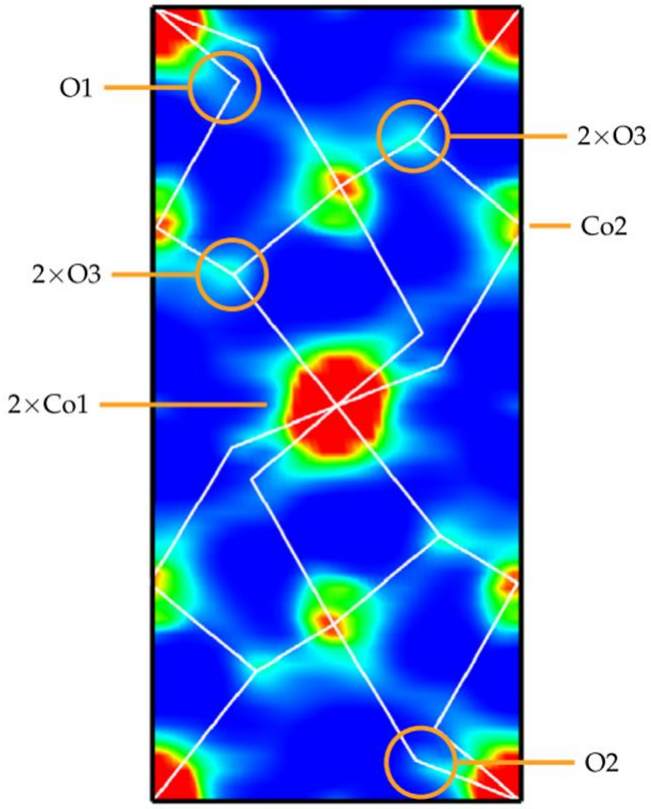

Fig. 8.14: *Reconstruction of the density (projected along the b axis) corresponding to the observed magnetization distribution of Co_2SiO_4 at 70 K with contours ranging from 0 $\mu_B/Å^3$ (blue) to 2 $\mu_B/Å^3$ (red) [4].*

Among the interesting features of this map is the observation of magnetization density on the, nominally non-magnetic, oxygen atoms coordinating the Co^{2+}-ions. These 'transferred moments' are direct experimental evidence for the hybridization of the oxygen 2p- with Co-3d-orbitals which is not only responsible for covalent bonding but also for the magnetic exchange interaction along the Co-O-Co-bond network.

References

[1] W. Reimers, E. Hellner, W. Treutmann and G. Heger, J. Phys. C: Solid State Phys. **15**, 3597 (1982).

[2] R. J. Nelmes, W. F. Kuhs, C. J. Howard, J. E. Tibballs and T. W. Ryan, J. Phys. C: Solid State Phys. **18**, L711 (1985).

[3] S. Mattauch, G. Heger, and K. H. Michel, Cryst. Res. Technol. **39**, 1027 (2004)

[4] A. Sazonov, Ph.D.-thesis, RWTH Aachen (2009)
A. Sazonov et al., Acta Cryst. **B65**, 664-675 (2009).

Exercises

E8.1 Rietveld refinement

A. What is the basic problem in refining crystal structures from powder diffraction data?

B. Sketch the fundamental idea to solve this problem.

C. What kind of data can be obtained from a Rietveld refinement?
(collect a list and sort into categories: Structural parameters, instrumental parameters, others)
D. Can powder diffraction data be used for structure determination? *(yes or no plus arguments)*

E8.2 Thermal displacement Parameters

A. Write down the (isotropic) displacement factor ("Debye-Waller-factor") that enters the structure factor formula (for x-rays)

B. Discuss the physical origin of this factor.

C. Describe the overall effect of this displacement factor on the diffracted intensities.

D. Do you expect the formal description to be fundamentally different for neutron diffraction as compared to x-ray diffraction?

E. It is generally said, that neutron diffraction yields much more precise displacement parameters than x-ray diffraction. Correct? If so: Why?

F. What are anisotropic displacement parameters and how can they be visualized?

G. Is it correct, that all atoms in cubic crystals have to vibrate isotropically?

H. Discuss the symmetry restrictions (shape and orientation of the ellipsoid) following from the point symmetry at the atomic sites for the following cases: **-1**, **2/m**, **4/m -3 2/m**

E8.3 Displacements at low temperatures

A. Discuss the reduction of the displacement parameters with decreasing temperature (fig.8.8): Is this effect real or an artefact? Arguments?

B. Discuss the non-zero values of the displacements factors for T => 0 K in the same figure and the different values for different atom types.

E8.4 Choice of neutron wavelengths

A. Magnetic neutron diffraction experiments are usually done with rather long wavelengths (see chapter 8.7: λ = 1.87 Å): Why?

B. Diffraction experiments aiming at obtaining precise atomic coordinates and displacements are done with much shorter wavelengths (see chapter 8.8: λ = 0.552 Å): Why?

C. Powder diffraction experiments usually use longer wavelengths than single crystal experiments: Why?
(Discuss this issue in terms of the competition between angular and direct space resolution.)

E8.5 Density maps from diffraction experiments

A. How can one obtain (from diffraction) the bonding electron density map?
(discuss the experiment(s), the necessary calculations and the information obtained)

B. Discuss the difference between the bonding electron density map and a magnetization density map. *(which kind of data is used, what is the specific information?)*

E8.6 Hydrogen bonded crystals

Assume you have grown a new hydrogen-bonded compound in the form of a single crystal and you want to know how the hydrogen bonds are arranged within the structure.

A. Collect arguments pro & con the usage of single crystal x-ray- vs. neutron diffraction experiment to study your new crystal.
(Discuss availability / costs of the experiment, required size of the crystal, scattering power of hydrogen, absorption & incoherent scattering, additional effort to deuterate etc.)